

Radiative interaction between the relativistic jet and optically thick envelope in tidal disruption events

Wenbin Lu^{1*}, Julian Krolik^{2†}, Patrick Crumley³, Pawan Kumar¹

¹*Department of Astronomy, University of Texas at Austin, Austin, TX 78712, USA*

²*Physics and Astronomy Department, Johns Hopkins University, Baltimore, MD 21218, USA*

³*Anton Pannekoek Institute for Astronomy, University of Amsterdam, PO Box 94249, NL-1090 GE Amsterdam, the Netherlands*

5 November 2021

ABSTRACT

Reverberation observations yielding a lag spectrum have uncovered an Fe $K\alpha$ fluorescence line in the tidal disruption event (TDE) Swift J1644+57 (Kara et al. 2016). The discovery paper used the lag spectrum to argue that the source of the X-ray continuum was located very close to the blackhole (~ 30 gravitational radii) and moved sub-relativistically. We reanalyze the lag spectrum, pointing out that dilution effects cause it to indicate a geometric scale an order of magnitude larger than inferred by Kara et al. (2016). If the X-ray continuum is produced by a relativistic jet, as suggested by the rapid variability, high luminosity and hard spectrum, this larger scale predicts an Fe ionization state consistent with efficient $K\alpha$ photon production. Moreover, the momentum of the jet X-rays impinging on the surrounding accretion flow on this large scale accelerates a layer of gas to speeds $\sim 0.1\text{--}0.2c$, consistent with the blueshifted line profile.

Implications of our results on the global picture of jetted TDEs are discussed. A power-law γ /X-ray spectrum may be produced by external UV-optical photons being repetitively inverse-Compton scattered by *cold* electrons in the jet, although our model for the $K\alpha$ reverberation does not depend on the jet radiation mechanism (magnetic reconnection in a Poynting jet is still a viable mechanism). The non-relativistic wind driven by jet radiation may explain the late-time radio rebrightening in Swift J1644+57. This energy injection may also cause the thermal UV-optical emission from jetted TDEs to be systematically brighter than in non-jetted ones.

Key words: galaxies: nuclei — accretion, accretion disks — methods: analytical

1 INTRODUCTION

A new type of γ /X-ray transients—tidal disruption events (TDEs) with jets—was established by the discovery of Swift J164449.3+573451 (hereafter Swift J1644+57, Bloom et al. 2011; Burrows et al. 2011; Levan et al. 2011; Zauderer et al. 2011), Swift J2058.4+0516 (hereafter Swift J2058+05, Cenko et al. 2012) and possibly a third one Swift J1112.2+8238 (Brown et al. 2015). They are observationally different from other non-jetted TDEs discovered in the UV-optical band (e.g. Gezari et al. 2009, 2012; Arcavi et al. 2014; Holoien et al. 2016; Hung et al. 2017) and soft X-ray band (e.g. Komossa et al. 2004; Saxton et al. 2012, 2016) in that they are much brighter, have harder X-ray spectra and vary on much shorter timescales (Bloom et al. 2011).

The generic model for TDEs is that they begin when a star with mass M_* and radius R_* falls toward a supermassive blackhole (BH) of mass $M = 10^6 M_6 M_\odot$ along a parabolic orbit with pericenter distance smaller than the tidal disruption radius R_T , a distance determined by matching the BH's tidal forces to the star's self gravity

$$R_T \simeq R_* \left(\frac{M}{M_*} \right)^{1/3}, \quad (1)$$

which is $\simeq (7.0 \times 10^{12} \text{ cm}) M_6^{1/3} (M_*/M_\odot)^{-1/3} (R_*/R_\odot)$ for a main-sequence star.

The initial condition for a TDE is very simple, but the dynamics after disruption are extremely complicated due to the 3 dimensional nature and the wide range of time-/length-scales involved. Because constructing a global deterministic model is a formidable task, various analytical and numerical calculations have been carried out studying different aspects of the post-disruption physics, e.g. fall-back

* wenbinlu@astro.as.utexas.edu

† jhk@jhu.edu

stream evolution (e.g. Kochanek 1994; Lodato et al. 2009; Stone et al. 2013; Guillochon & Ramirez-Ruiz 2013, 2015; Coughlin et al. 2016), stream-stream collisions (Jiang et al. 2016), stream magnetization (Guillochon & McCourt 2016; Bonnerot et al. 2016), disk formation (Shiokawa et al. 2015; Bonnerot et al. 2016; Sądowski et al. 2016), disk evolution (Shen & Matzner 2014; Piran et al. 2015a), possible large-scale envelope inflation (Loeb & Ulmer 1997; Coughlin & Begelman 2014), super-Eddington disk winds (Strubbe & Quataert 2009; Metzger & Stone 2016), jet propagation (De Colle et al. 2012), and unbound debris evolution (Guillochon et al. 2016; Krolik et al. 2016). Many of these studies are very recent and this subject is developing rapidly.

Since different dynamical processes are deeply interconnected, it is crucial to put together different pieces of observations to understand the bigger picture (e.g. Krolik et al. 2016). The three most distinct observational components of a jetted TDE are: non-thermal γ /X-ray emission, thermal UV-optical emission, and non-thermal radio/mm emission. The first is often thought to be the result of internal dissipation within a jet; the second is sometimes identified with the surface of the accretion flow and sometimes with a reprocessing outflow; the third is generally attributed to external shocks formed when an outflow runs into the circum-nuclear medium. In this paper, we propose that the radiation from the jet, upon striking the accretion flow, can drive a kind of outflow not previously considered.

Swift J1644+57, at redshift $z = 0.354$ (Levan et al. 2011), has a rich set of data in terms of time (minutes to years) and multi-wavelength (radio to γ -rays) coverage; see the referenced discovery papers. The non-thermal γ /X-ray emission had averaged¹ isotropic luminosities 10^{47} - 10^{48} erg s⁻¹ in the first 10 d (hereafter host-galaxy rest frame time) and then declined roughly as $t^{-5/3}$ until a sudden drop at about 370 d (Zauderer et al. 2013; Mangano et al. 2016). The X-ray lightcurve showed very fast variability with a minimum variability timescale $\simeq 78$ s (host-galaxy rest frame time). The observed X-ray spectrum for Swift J1644+57 by *Swift*/XRT in the $0.3(1+z)$ - $10(1+z)$ keV range was a power-law $F_\nu \propto \nu^{-\alpha}$ with early time (25-86 d) spectral index $\alpha \simeq 0.8$ and late time (~ 100 d) $\alpha \simeq 0.5$ (Saxton et al. 2012). The early time spectrum extends up to $150(1+z)$ keV without a break (Burrows et al. 2011). Therefore, most of the radiation energy is on the high frequency end, which possibly extends to the electron rest-mass energy or higher.

Unfortunately, due to the large dust extinction $A_V \sim 10$ mag, Swift J1644+57 was not observable in the UV where the peak of the thermal disk/envelope emission is predicted to be (e.g. Loeb & Ulmer 1997). After correcting for dust extinction, the thermal component can be seen in the near-infrared (Levan et al. 2016). Swift J2058+05 was similar to

Swift J1644+57 in the X-ray band² but had much less dust extinction ($A_V \sim 0.5$ mag, Cenko et al. 2012). The thermal UV-optical emission from Swift J2058+05 was observable up to 60 days after discovery (Pasham et al. 2015). We call the source of the thermal UV-optical component the *envelope* in general, which could be a thick disk or quasi-spherical envelope inflated by radiation pressure (Loeb & Ulmer 1997; Coughlin & Begelman 2014), an optically thick wind launched from the disk (Metzger & Stone 2016), or the shock from stream-stream collisions (Piran et al. 2015b). It is widely known that the photospheric radii of the thermal UV-optical emission in TDEs are much larger than the tidal disruption radius given by eq. (1); see the referenced TDE discovery papers and we also provide a simple estimate in Appendix A. We point out that, if the conversion from jet energy to radiation occurs below the photosphere of the envelope, the jet radiation will likely interact with and affect the dynamics of the envelope.

An evidence of this interaction is the Fe K α line detected in Swift J1644+57 by *XMM-Newton* at ~ 14 d (and possibly also by *Suzaku* at ~ 7 d) post-discovery (Kara et al. 2016). The flux variations of the Fe K α line in the frequency range $(2-10)(1+z) \times 10^{-4}$ Hz followed the corresponding variations in the continuum at 4-5 keV and 8-13 keV with a lag time of $\sim 120/(1+z)$ s. This is most naturally explained by fluorescence of the jet X-rays off an ionized reflector. The peak of the lag-energy spectrum is at $\simeq 8$ keV, which corresponds to a line-of-sight (LOS) velocity $\simeq 0.1-0.2c$, considering the rest line energy between 6.4 and 6.97 keV (depending on the ionization state of Fe). Since we are viewing the system at a low inclination (with the jet axis close to our LOS), such a high velocity is hard to associate with the rotation of a disk, so the reflector must be an outflow moving away from the disk toward us (see a schematic picture in Fig. 1).

In this paper, we study the interaction between jet radiation and the surrounding envelope and discuss how this interaction affects the dynamics of the envelope and implications on the global picture of jetted TDEs. In section 2, we discuss the physical constraints on the jet Lorentz factor and show that the jet is moving at a relativistic speed. In section 3, we discuss the physical state of the envelope based on observations of Swift J2058+05, a close analog to Swift J1644+57. In section 4 and 5, we study how the observed K α line is produced in the jet-envelope interaction. Implications of our results and some possible issues are discussed in section 6. A short summary is in section 7. Unless otherwise clearly stated, all frequencies, time and luminosities in this paper have been de-redshifted to the host-galaxy rest frame (for Swift J1644+57 at $z = 0.354$). Throughout the paper, the convention $Q = 10^n Q_n$ and CGS units are used.

2 RELATIVISTIC MOTION OF THE JET

In this section, we derive a conservative lower limit of the bulk Lorentz factor of the γ /X-ray emitting plasma from simple Compton scattering arguments. The radiation seen

¹ In the first a few days, the γ /X-ray lightcurve of Swift J1644+57 had multiple hard flares, with rise time ~ 100 s, flare duration ~ 1000 s and quiescent interval $\sim 5 \times 10^4$ s. These properties have been attributed to the disruption of a white dwarf (by an intermediate-mass BH) instead of a main-sequence star (Krolik & Piran 2011). Our analysis in this paper deals with processes happening at large radii $\gtrsim 10^{13}$ cm and is hence insensitive to the nature of the disrupted star and the BH mass.

² Unfortunately, Swift J2058+05 is much farther away (by a factor of ~ 4) and no reverberation observation was carried out.

by the observer is also impinging and exerting a Compton force on electrons in the (optically thin) source. This is equivalent to the case where an electron is at a distance R from a point source of the same luminosity.

Let this electron move with speed β (Lorentz factor $\Gamma = (1 - \beta^2)^{-1/2}$) radially outward from an isotropic radiation source of L . For a baryonic jet, the electron, with the inertia of a proton m_p , experiences an acceleration from Compton scattering

$$\frac{dp'}{dt'} = \Gamma^2(1 - \beta)^2 \frac{L\sigma_T}{4\pi R^2 c}, \quad (2)$$

where the momentum and time in the electron's comoving frame are denoted with a prime ($'$) and the R.H.S. is the momentum flux in the comoving frame multiplied by the Thomson cross section σ_T . Going back to the rest frame of the BH, it can be shown that $dp'/dt' = m_p c d(\Gamma\beta)/dt$.

Using $dR = \beta c dt$, $R = 10^{13} R_{13}$ cm and $L = 10^{47} L_{47}$ erg s $^{-1}$, we obtain

$$\frac{\Gamma\beta d\beta}{(1 - \beta)^2} = 11.8 L_{47} \frac{dR_{13}}{R_{13}}, \quad (3)$$

which can be integrated analytically. For initial condition $\beta = 0$, an electron accelerated from R to $2R$ attains a Lorentz factor given by

$$\frac{2\beta - 1}{3\Gamma(1 - \beta)^2} = 5.9 \frac{L_{47}}{R_{13}} - \frac{1}{3}. \quad (4)$$

With bolometric correction of a factor of a few, the typical γ /X-ray luminosity of Swift J1644+57 within the first ~ 10 days is $L \simeq 3 \times 10^{47}$ erg s $^{-1}$, so an electron accelerated from R to $2R$ attains a Lorentz factor of $\Gamma = (2.6, 1.9, 1.5, 1.3)$ when $R = (1, 3, 10, 20) \times 10^{13}$ cm. These are conservative lower limits for the jet Lorentz factor at the radius where γ /X-rays are produced.

The X-ray emission from Swift J1644+57 had a minimum variability timescale $t_{\text{var},\text{min}} = 78$ s. If the X-ray source is moving at Lorentz factor Γ toward the Earth and the comoving size of the emitting region is R/Γ (the causally connected region), the jet radiation radius can be estimated by (Bloom et al. 2011)

$$R \simeq \Gamma^2 c t_{\text{var},\text{min}} = 2.3 \times 10^{12} \Gamma^2 \text{ cm}. \quad (5)$$

Combining eqs. (4) and (5), one obtains $\Gamma \simeq 2.4$, which may be considered as a lower limit of the Lorentz factor at the radius where the jet is radiating.

Note that the variability timescale could be affected by many factors (e.g. the comoving size of the emitting region could be much smaller than R/Γ), so we do not use $t_{\text{var},\text{min}}$ as a hard constraint on the relation between R and Γ . We also note that, for a baryonic jet with hot electrons (electrons' Lorentz factors in the comoving frame $\gamma_e > 1$) or with lepton-to-proton number ratio larger than 1, the lower limit on Γ will be stronger.

On the other hand, if the jet is Poynting-dominated and the lepton-loading is very low, the effective inertia of an electron could be larger than m_p , so Compton acceleration may not be efficient³. However, the jet will accelerate as a result

of its own magnetic pressure gradient. The fast X-ray variability implies that the jet is not continuous but intermittent with individual ‘‘blobs’’ likely having durations $t_0 \lesssim t_{\text{var},\text{min}}$. If the initial magnetization of such a blob $\sigma_0 \gg 1$, it quickly accelerates to a Lorentz factor $\Gamma \simeq \sigma_0^{1/3}$ after propagating a distance of $R_0 \sim ct_0 \lesssim 2.3 \times 10^{12}$ cm, and then the Lorentz factor increases with radius R as $\Gamma \sim (\sigma_0 R/R_0)^{1/3}$ until the saturation radius $R_s \simeq \sigma_0^2 R_0$ (Granot et al. 2011). For instance, for $\sigma_0 \simeq 10$, the jet in Swift J1644+57 can accelerate to $\Gamma \gtrsim 5$ at $\sim 10^{13}$ cm from the BH. The acceleration could be even faster when there is extra collimation. Komissarov et al. (2007) show that for $\sigma_0 \simeq 10$, Poynting-dominated jets accelerate to $\Gamma \simeq 5$ at $10\text{--}30 R_{\text{lc}}$, where $R_{\text{lc}} \simeq 4R_g$ is the light cylinder radius of a fast spinning ($a \simeq 1$) Kerr BH and $R_g = GM/c^2$ is the gravitational radius.

We also note that the early time γ /X-ray spectrum of Swift J1644+57 is a power-law $F_\nu \propto \nu^{-\alpha}$ ($\alpha \simeq 0.8$) extending up to 200 keV without a break (Burrows et al. 2011; Bloom et al. 2011). If this power-law continues extending up by a factor of a few to \sim MeV energy, relativistic motion is needed to alleviate the compactness problem. For example, for luminosity $\nu L_\nu|_{\text{MeV}} \simeq 10^{47}$ erg s $^{-1}$ and minimum variability time $t_{\text{var},\text{min}} \simeq 10^2$ s, the optical depth for pair production reaches $\tau_{\gamma\gamma} \sim 10^5$, which can be reduced by a factor of $\Gamma^{-6+2\alpha}$ if the source is moving toward the Earth at Lorentz factor Γ .

Another argument for a relativistic jet is that, when the X-ray source is non-relativistic, Fe ions are fully stripped and hence $K\alpha$ production is strongly suppressed (see section 4).

3 PHYSICAL STATE OF THE ENVELOPE

In this section, we discuss the physical properties of the thermal UV-optical source. We call it the *envelope* because it wraps around the relativistic jet. This region is the presumptive source of $K\alpha$ photons. We discuss its temperature, photospheric radius, density, pressure, etc. Interaction between jet radiation and the envelope will be discussed in the next section.

When the bound stellar mass returns to the vicinity of the BH, several shock systems are formed (Shiokawa et al. 2015). One, the ‘‘nozzle shock’’, forms near the stellar pericenter as debris streams converge toward the orbital plane; this shock deflects a minority of the bound mass in toward the BH, while a majority of the material continues along the highly-elliptical orbits. Other shocks form where the streams intersect in the orbital plane. If the stellar pericenter $R_p \gtrsim 10R_g$ (where $R_g \equiv GM/c^2$), these shocks are near the apocenters of the stream orbits, ultimately creating an extended accretion flow on the scale of the semi-major axis of the most-bound debris, $\sim (M/M_*)^{1/3} R_T$. On the other hand, if the stellar pericenter $R_p \lesssim 10R_g$, relativistic apsidal precession is strong enough to bring those shocks in to radii not much greater than R_p (Dai et al. 2015). Because the in-plane shocks dissipate an amount of energy comparable

³ Poynting-dominated jets could be dissipative over certain range of distances from the central engine. The following two reasons could lead to a larger acceleration: (1) an outward gradient

of magnetic pressure when dissipation causes magnetic energy to decrease with distance (e.g. Drenkhahn & Spruit 2002); (2) the Compton rocket effect when leptons are accelerated to high Lorentz factors in the comoving frame (e.g. Odell 1981; Phinney 1982).

to the binding energy of the orbit, and the cooling time is generally comparable to or longer than the orbital timescale (Piran et al. 2015b), the resulting structure is geometrically thick. However, because some of its support remains rotational, a cone aligned with the angular momentum axis is left almost clear of gas (this picture is complicated by Lense-Thirring dynamics, a point we neglect for the time being). If our viewing angle lies within the opening angle of the cone, the likely state when we are seeing radiation from a jet, we can see the inner surface of this cone directly.

The radial scale on which the majority of the mass is distributed can be estimated in two ways. One is the semi-major axis scale of the most-bound debris already mentioned. Another is phenomenological, by identifying the UV-optical emission with thermal radiation from the photosphere of the optically thick gas and measuring (or at least constraining) its temperature from the observed spectrum. This latter method may have large uncertainty when applied to Swift J1644+57 because of its large extinction (we provide a rough estimate in Appendix A). On the other hand, if we suppose that other TDEs can be used as stand-ins for Swift J1644+57, it can be applied to them. In the case of many ordinary “thermal” non-jetted TDEs, this method yields radial scales quite consistent with the semi-major axis estimate (Piran et al. 2015b); see also Appendix A for simple estimates.

Perhaps a closer analog to Swift J1644+57, however, is Swift J2058+05, whose output was similarly dominated by hard X-rays. In this case, UV-optical continuum was detected, but the thermal component was entirely in the Rayleigh-Jeans (R-J) limit, and could therefore place only a lower bound on the temperature $kT > h\nu_0$ (ν_0 being the detection frequency). We may place an upper bound on the radiating area of Swift J2058+05 because the specific luminosity from a thermal surface in the R-J limit is $L_{\nu_0} \propto R_{\text{ph}}^2 \nu_0^2 T$. For Swift J2058+05, the specific luminosity at $\nu_0 = 1.0 \times 10^{15}$ Hz is $\nu_0 L_{\nu_0} = 1.3 \times 10^{44}$ erg s⁻¹ (Pasham et al. 2015) about 11 days post discovery, and then this argument implies a radial scale at most $\sim 5 \times 10^{14}$ cm. On the other hand, the bolometric luminosity from a thermal surface is $L_{\text{bol}} \propto R_{\text{ph}}^2 T^4$ and it should be less than $\sim 10^{47}$ erg s⁻¹ given by the total energy budget⁴ of $\sim 10^{53}$ erg and duration $\sim 10^6$ s. This argument gives a radial scale at least $\sim 2 \times 10^{14}$ cm. Although these arguments are based on spherical-symmetry assumption, we do get a good insight on the radial scale of the thermal envelope being a few $\times 10^{14}$ cm.

This radial scale estimate describes Swift J2058+05, but we will henceforward adopt 10^{14} cm as a fiducial radial scale for the accretion flow around Swift J1644+57. In terms of this fiducial scale, we can make several estimates defining characteristic conditions of the bound gas of total mass M_b . Assuming solar metallicity with Thomson opacity $\kappa_T = 0.34$ cm² g⁻¹, we have the Thomson optical depth $\tau_T \simeq 2 \times 10^3 (M_b/0.4M_\odot) R_{14}^{-2}$ and mean mass density

$$\bar{\rho} \simeq (2 \times 10^{-10} \text{ g cm}^{-3}) (M_b/0.4M_\odot) R_{14}^{-3}, \quad (6)$$

⁴ About half of the star remains bound and about half of the bound mass falls back within the Keplerian period of the most bound orbit. Other processes, e.g. adiabatic expansion and accretion efficiency being less than unity, will likely reduce the radiation energy to $\sim 10\%$ of the total rest mass energy available.

implying an electron number density of $\bar{n}_e \simeq (1 \times 10^{14} \text{ cm}^{-3}) (M_b/0.4M_\odot) R_{14}^{-3}$. For photons with energy near kT , the bound-free opacity, which dominates over free-free opacity in the temperature and density ranges of interest, is $\kappa_{\text{bf}} \simeq (0.4 \text{ cm}^2 \text{ g}^{-1}) T_5^{-7/2} (M_b/0.4M_\odot) R_{14}^{-3}$, which is comparable to the Thomson opacity κ_T . We scale here to a temperature of 10^5 K to be consistent with the R-J character of the Swift J2058+05 UV-optical spectrum ($T \gtrsim 6 \times 10^4$ K, Cenko et al. 2012). Also for Swift J2058+05, the energy budget constraint $L_{\text{bol}} \lesssim 10^{47}$ erg s⁻¹ restricts the temperature to be $T \lesssim 2.5 \times 10^5$ K.

In these conditions, radiation pressure $aT^4/3 \simeq 2 \times 10^5 T_5^4$ dyne cm⁻² (a being the radiation constant) dominates over gas pressure $1.4\bar{\rho}kT/m_p \simeq (2 \times 10^3 \text{ dyne cm}^{-2}) T_5 (M_b/0.4M_\odot) R_{14}^{-3}$. If the isotropic equivalent X-ray luminosity $L_X \sim 10^{47}$ erg s⁻¹ were aimed along the normal to the inner surface of the gas cone, it would exert a pressure $\sim 3 \times 10^7 R_{14}^{-2}$ dyne cm⁻², much greater than either the gas or thermal radiation pressure we have estimated. However, if the jet is both relativistic and runs along the axis of the open cone, the flux striking the surrounding gas is reduced relative to its maximally beamed value by both relativistic beaming and geometric projection. For a relativistic point source with spectrum $F_\nu \propto \nu^{-\alpha}$ ($\alpha \simeq 0.8$ in the first a few weeks, Burrows et al. 2011; Bloom et al. 2011), the reduction due to the former is $\simeq [\Gamma^2(1 - \beta \cos \theta)]^{-(3+\alpha)}$ in the polar-angle direction θ from a jet traveling at βc and Lorentz factor $\Gamma \gg 1$; the latter is $\cos \psi$, where ψ is the angle between the ray direction from the source to the surface and the surface normal. It is also possible that the flux incident on the surrounding gas can be augmented at order-unity level by X-rays that are reflected by the one part on the inner cone surface and then strike again somewhere else across the cone. The reduction in pressure is another factor of $\cos \psi$ times the reduction in flux. The location of the cone surface may be determined by pressure balance from the jet radiation, centrifugal force, gravity and the intrinsic gas thermal pressure. A schematic picture of the transition region between the jet and the optically thick envelope is shown in Fig. (1).

4 IRON K α EMISSION LINE

Knowing the properties of the surrounding envelope, we discuss the conditions required to produce a K α line consistent with observations. We focus on the ionization state of Fe (§4.1) and equivalent width (§4.2) and broadening (§4.3) of the K α line. At the end (§4.4), we propose that the momentum of the jet X-rays impinging on the envelope accelerates a layer of gas to speeds $\sim 0.1\text{--}0.2c$, consistent with the observed blueshift. Lag time will be discussed in section 5.

4.1 Ionization state of Fe

Kara et al. (2016) reported a detection of an Fe K α emission line in the lag-energy spectrum from Swift J1644+57 and explained it as due to fluorescence from an outflowing funnel wall exposed to X-rays from a sub-relativistically moving source close to the BH. The lag-energy spectrum related variations of the line flux and the continuum over the

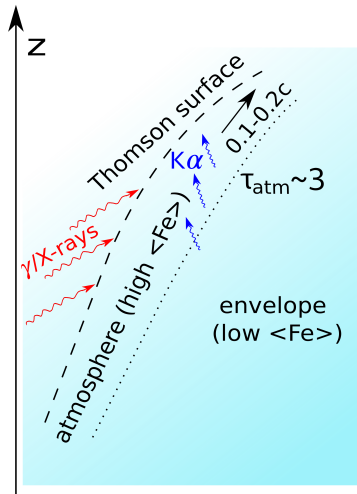


Figure 1. Schematic picture of the transition region between the jet and the optically thick envelope. The γ /X-rays from the jet (in red wiggly lines) impinge on the optically thick envelope (light blue region). The surface where the Thomson depth of the envelope $\tau = 1$ is called the *Thomson surface* and denoted by a black dashed curve. The part of the envelope with Thomson depth $\tau_{\text{atm}} \sim 3$ where the γ /X-rays can diffuse to is called the *atmosphere*. The mean value of the Fe ionization state $\langle Fe \rangle$, i.e. the averaged number of positive charges per Fe ion, decreases as we go deeper into the envelope. We show in §4.1 that the conditions such that Fe ions have a few bound electrons can be realized in the atmosphere, so $K\alpha$ line photons (in blue wiggly lines) can be naturally produced in those regions. We also show in §4.3 that the atmosphere can be accelerated to speeds $\sim 0.1-0.2c$ by the momentum kick from the incident γ /X-rays.

frequency range $(2-10)(1+z) \times 10^{-4}$ Hz, and the observed peak lag was $\sim 120/(1+z)$ s.

In their kinematical toy model, the X-ray source is stationary at a point on the funnel axis $30R_g$ from the BH, the funnel opening angle is $30-45^\circ$, and the gas at the funnel wall accelerates radially outward from $0.1c$ to $\sim 0.5c$. The wall fluoresces from $6R_g$ out to $200R_g$. They also suggest a BH mass of $2 \times 10^6 M_\odot$, which places the X-ray source at 9×10^{12} cm from the BH.

However, this model is problematic in several ways. The first has to do with the ionization state of the gas at the funnel wall. Since the X-rays are emitted isotropically in the model, the luminosity per unit solid angle incident on the funnel is the same as we see, $L_X = 4\pi dL_X/d\Omega = 10^{47} L_{X,47}$ erg s $^{-1}$ in the $0.3(1+z)-10(1+z)$ keV band. If we focus on ionization of H-like Fe (Fe^{25+}), the threshold energy is $h\nu_{\text{th}} = 9.3$ keV, so only the portion of the spectrum above that energy is relevant. The observed spectral slope $L_\nu \propto \nu^{-0.8}$ leads to a luminosity $\nu L_\nu|_{\nu_{\text{th}}} = 0.37L_X$ at the threshold energy. With the assumption that the distance from the BH to the X-ray source ($\sim 10^{13}$ cm) is the same as the characteristic distance from the source to the funnel (a good approximation for this conical geometry), the X-ray flux incident on the funnel is $\nu F_\nu|_{\nu_{\text{th}}} \simeq 3 \times 10^{19}$ erg cm $^{-2}$.

Then, the photoionization timescale for Fe^{25+} is

$$t_{\text{pi}} = \left(\int_{\nu_{\text{th}}}^{\infty} \sigma_{\text{pi}}(\nu) \frac{F_\nu}{h\nu} d\nu \right)^{-1} = \frac{(3+\alpha)h\nu_{\text{th}}}{\sigma_{\text{pi,th}}(\nu F_\nu|_{\nu_{\text{th}}})} \quad (7)$$

$$\simeq (6 \times 10^{-8} \text{ s}) L_{X,47}^{-1}$$

where we have used the photoionization cross section $\sigma(\nu) = \sigma_{\text{pi,th}}(\nu/\nu_{\text{th}})^{-3}$ and $\sigma_{\text{pi,th}} \simeq 3.3 \times 10^{-20}$ cm 2 for Fe^{25+} (George & Fabian 1991). On the other hand, the recombination timescale from Fe^{26+} to Fe^{25+} is

$$t_{\text{rec}} \simeq (\alpha_A n_e)^{-1} \simeq (5 \times 10^{-5} \text{ s}) (\rho/\bar{\rho})^{-1} T_5^{0.7}, \quad (8)$$

where we have used the Case A recombination rate coefficient $\alpha_A \simeq (2.0 \times 10^{-10} \text{ cm}^3 \text{ s}^{-1}) T_5^{-0.7}$ (Draine 2011) and the mean density $\bar{\rho}$ estimated in eq. (6). Comparing eq. (7) with eq. (8), we see that only $\sim 10^{-3}$ of all Fe ions retain even a single electron, and the $K\alpha$ production rate is correspondingly suppressed. Note that we previously justified an estimated temperature for the funnel wall of $\sim 10^5$ K on the grounds that it had to be hot enough to make the UV-optical continuum of Swift J2058+05 entirely within the Rayleigh-Jeans range; strong photoionization can drive the temperature to at least this level.

Second, from section 2, we know that a baryonic dominated source will be accelerated by the radiation pressure to Lorentz factors $\Gamma \gtrsim 2.5$ for if the γ /X-rays are produced at $R \lesssim 10^{13}$ cm. A magnetic energy dominated source will also accelerate to relativistic speeds due to its own magnetic pressure gradient. Moreover, as we have shown in section 3, for a sub-relativistic source from which γ /X-rays are emitted nearly isotropically, the radiation pressure of the γ /X-rays will push the envelope out to much greater distance, vitiating the lag-time argument in Kara et al. (2016).

Third, it is unclear how a sub-relativistic source can produce a hard γ /X-ray spectrum (Burrows et al. 2011; Bloom et al. 2011), given that the source is suffused by a large injection of thermal seed photons from the surrounding envelope.

All the problems in the model of Kara et al. (2016) can be solved readily by two modifications: (i) moving the radial scale of the fluorescing matter outward by an order of magnitude, to the scale suggested by tidal disruption dynamics, and (ii) putting the source of γ /X-rays in a relativistic jet. We will reconcile the latter change with the lag spectrum in section 5.

Moving the fluorescing matter to a radius 10 times greater ($\sim 10^{14}$ cm) reduces the flux by a factor of $\sim 10^{-2} \cos \psi$, where $\psi \gtrsim 60^\circ$ is the angle between X-ray direction and the surface normal (see Fig. 2). If the γ /X-ray source is, in fact, a relativistic jet, then the flux on the envelope surface can be reduced by an additional factor of $\eta_{\text{rel}} \lesssim 0.1/(\cos \psi)$ by placing the surface outside the relativistic beaming cone. As shown later in §4.2, this reduction factor is related to the $K\alpha$ equivalent width and is consistent with observations. Combining these two effects, the photoionization timescale can easily rise to be comparable to or greater than the recombination time, so that most Fe ions retain at least one electron. As already remarked, the same reduction in flux due to jet-beaming also permits an equilibrium between the X-ray radiation pressure and the envelope pressure. Lastly, bulk Comptonization can lift the thermal UV-optical photons from the surrounding envelope to the X-ray band without requiring relativistic electrons in the comoving frame of the source.

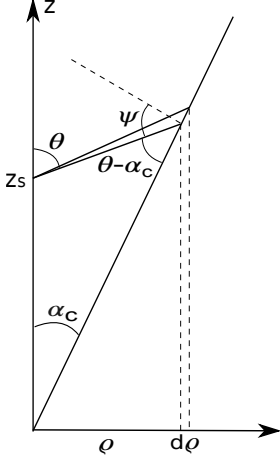


Figure 2. Conical inner surface geometry. The X-ray source is on the z -axis at z_s . The polar angle of the inner surface of the envelope is α_c . We denote the polar angle of light rays from the source as θ and the cylindrical radius of the illuminated point on the inner surface as ϱ . The relation between z_s and ϱ is given by $\cot \theta = \cot \alpha_c - z_s/\varrho$. The angle between light rays from the source and the surface normal is $\psi = \pi/2 - (\theta - \alpha_c)$.

In a more exact treatment, it would be necessary to consider more carefully the finite-thickness transition layer between the bulk of the surrounding gas and the low-density region within the cone. In that transition layer, the density declines below the mean, lengthening the recombination time. Determining the sharpness of this density cut-off is beyond the scope of the present work. We only comment that the density profile is probably not exponential because it is not determined by balancing a pressure gradient with gravity; instead, the principal mechanism is penetration of γ /X-rays into the gas layer and consequent heating. For this reason, its characteristic thickness is likely determined by the mean free path for Compton scattering. Thus, under these circumstances, the fluorescence efficiency should be fairly high.

4.2 $K\alpha$ equivalent width

Given a geometry for the envelope's inner surface, the equivalent width (EW) of the line can be readily calculated. For example, consider a simple model shown in Fig. (2) in which the inner surface is exactly conical, with half-opening angle α_c , and we have

$$EW = 2\epsilon_{K\alpha} Y \int \frac{d\varrho}{\varrho} \eta_{\text{rel}}(\theta) \sin^2 \theta \sin(\theta - \alpha_c) \int_{\frac{\epsilon_K}{\epsilon_{K\alpha}}} \frac{dx}{x^{1+\alpha}} f(\epsilon),$$

$$\simeq 2\epsilon_{K\alpha} Y f(\epsilon_K) \int \frac{d\varrho}{\varrho} \eta_{\text{rel}}(\theta) \sin^2 \theta \sin(\theta - \alpha_c)$$
(9)

where $\theta(\varrho)$ is the polar angle of light rays from the source, ϱ is the cylindrical radius of the illuminated point on the inner surface of the envelope, $\eta_{\text{rel}}[\theta(\varrho)] \equiv [dL/d\Omega(\theta)]/(dL/d\Omega)_{\text{LOS}}$ is the ratio between the intensity striking on the surface and the intensity beamed along the LOS (which we assume to be along the jet axis), ϵ_K and

$\epsilon_{K\alpha}$ are the energies of K-edge and $K\alpha$ photons respectively, the dimensionless integration variable $x \equiv \epsilon/\epsilon_{K\alpha}$, $f(\epsilon)$ is the fraction of incident X-rays of energy ϵ that photoionize an Fe ion before escaping, Y is the fluorescent yield. In the second row of eq. (9), we have used $\int_{\epsilon_K/\epsilon_{K\alpha}} f(\epsilon)x^{-1-\alpha}dx \simeq f(\epsilon_K)$, for the continuum power-law index $\alpha \simeq 0.8$, $\epsilon_K/\epsilon_{K\alpha} \simeq 4/3$ and $f(\epsilon)$ being a relatively smooth function.

Then we put numbers into eq. (9): $\epsilon_{K\alpha} \simeq 7$ keV, $f(\epsilon_K) \sim 1^5$, $Y \simeq 0.6$ (atomic yield for $\text{Fe}^{23+,24+,25+}$, Krolik & Kallman 1987), and $d\varrho/\varrho \sim 1$. The trigonometry factor $\sin^2 \theta \sin(\theta - \alpha)$ is roughly 0.05 with uncertainty⁶ of a factor of $\lesssim 3$. Therefore, we obtain $EW \sim 400\bar{\eta}_{\text{rel}}$ eV, where $\bar{\eta}_{\text{rel}}$ is the X-ray intensity correction due to relativistic beaming averaged over the reprocessing surface. In eq. (9), we have only included the $K\alpha$ photons emitted directly from the reprocessing surface. If the opening angle of the funnel wall $\alpha_c \lesssim 30^\circ$, a large fraction of $K\alpha$ photons could bounce between the inner surface of the wall before eventually escaping. These reflected $K\alpha$ photons have lower energies and longer lags with respect to continuum variations than the photons that escape directly without reflection, and they produce the red wing in the lag-energy spectrum (see discussion later in §4.3).

Modeling the detailed production and radiative transfer of $K\alpha$ photons is out of the scope of the current work. Considering the purpose of this paper being understanding the broad-brush picture of the jet-envelope interaction in Swift J1644+57, we hereafter use the rough estimate $EW \sim 400\bar{\eta}_{\text{rel}}$ eV, which has uncertainty up to a factor of 3 mostly due to the unknown geometry of the system.

We argued in §4.1 that in order for most Fe atoms to be H-like or less-ionized, the intensity ratio due to relativistic beaming $\bar{\eta}_{\text{rel}} \lesssim 0.1/(\cos \psi)$, where $\psi = \pi/2 - (\theta - \alpha_c)$ may vary in the range $(60^\circ, 90^\circ)$ and hence $\cos \psi \lesssim 0.5$. This means that the EW of the $K\alpha$ line in Swift J1644+57 should be $\lesssim 80$ eV (note that a modest ratio $\bar{\eta}_{\text{rel}} \sim 0.2$ implies that typical values for $\theta(\varrho)$ are at most a few times $1/\Gamma$). In the time-integrated flux spectrum from *XMM-Newton*, there is a narrow peak at 8 keV (host-galaxy rest frame; this is roughly the same energy as the peak in the lag-energy spectrum) with an EW of 60 ± 10 eV (Kara et al. 2016), which agrees with our model.

However, this apparent agreement should be viewed cautiously. In *Suzaku* data taken 7 days earlier, the EW is < 7 eV (Kara et al. 2016), suggesting that the $K\alpha$ EW is subject to sizable fluctuations, perhaps caused by the system's changing geometry or Fe ionization state. As we will discuss in section 5, the $K\alpha$ EW plays an important role in interpreting the lag spectrum. Due to possible fluctuations, we do not take $EW \simeq 60$ eV as a hard constraint on the system's parameters, in order to be conservative. Future

⁵ For solar metallicity ($n_{\text{Fe}} \simeq 3.5 \times 10^{-5} n_{\text{H}}$), the K-edge absorption opacity κ_K nearly equals to the Thomson opacity κ_T , if all Fe ions are H-like (κ_K is larger for less ionized Fe). Compton scattering does not destroy photons. In the narrow jet-cone geometry of Swift J1644+57, a photon reflected from the funnel wall will most likely hit the other side of the inner surface and eventually gets absorbed.

⁶ For $(\theta = 20^\circ, \alpha = 10^\circ)$, we have $\sin^2 \theta \sin(\theta - \alpha) \simeq 0.02$; for $(\theta = 30^\circ, \alpha = 20^\circ)$, it is $\simeq 0.04$; for $(\theta = 30^\circ, \alpha = 10^\circ)$, it is $\simeq 0.09$; for $(\theta = 45^\circ, \alpha = 30^\circ)$, it is $\simeq 0.13$.

multi-epoch observations of more jetted TDEs may confirm or falsify the existence of such a narrow $K\alpha$ line.

If it is true, this narrow line gives interesting constraints on the differential velocity, electron temperature and optical depth of the line emitting region. (1) The full-width at half maximum (FWHM) in the flux spectrum is only ~ 0.2 keV, which, combined with the blueshift velocity $v \sim 0.1-0.2c$, means the velocity difference between different parts of the line emitting gas is only $\delta v/v \sim 20\%$. This means these $K\alpha$ photons are produced in a area where the gas has nearly uniform LOS velocity. (2) Compton scattering broadens the $K\alpha$ line due to thermal motion of electrons and electrons' recoil. The former is a symmetric Doppler broadening with $\text{FWHM} = \sqrt{8\ln 2}(kT_e/m_e c^2)^{1/2}\epsilon_0 \simeq (0.2 \text{ keV})T_{e,6}^{1/2}$, where we have used the rest line energy $\epsilon_0 \simeq 7$ keV. This means that the narrow line emitting region must have temperature $T_e \leq 10^6$ K. The latter (electrons' recoil) causes $K\alpha$ photons to consistently lose energy; $\epsilon_0^2/(m_e c^2) \simeq 0.1$ keV per scattering (assuming $4kT_e \ll \epsilon_0$). This means that the $K\alpha$ photons in this narrow line are produced in a region where the Thomson depth is $\tau \lesssim 2$.

4.3 Bouncing between the funnel wall surface

While the narrow line in the flux spectrum of *XMM-Newton* has FWHM ~ 0.2 keV, the line in the lag-energy spectrum is much broader, with FWHM ~ 1 keV⁷. We show that the broad red wing in the lag-energy spectrum is likely due to $K\alpha$ photons bouncing between the inner surface of the envelope.

In §4.2, we only considered thermal and Compton broadening within the $K\alpha$ emitting region. The average fractional energy loss of a photon in each Compton scattering is $\epsilon_0/(m_e c^2) \simeq 1.4\%$. In the physical situation, $K\alpha$ photons are produced at a range of optical depths $\tau \in (1, \sim 3)$, so we expect a narrow component from directly escaping photons which are only Doppler broadened due to different LOS velocities and a broad component which is broadened due to both Doppler effect and Compton scattering (see Fig. 14 of Pozdnyakov et al. 1983). A fraction of $K\alpha$ photons may scatter off electrons up to $\sim 5-10$ times (depending on τ at the emitting location), possibly causing broadening at the level of $\sim 10\%$ (or 1 keV) toward the red wing. Due to the small mean free path $(\kappa_T \rho)^{-1} \simeq 1.5 \times 10^{10}(\rho/\bar{\rho})^{-1}$ cm ($\bar{\rho}$ is the mean density of the envelope given by eq. 6), scattering within the $K\alpha$ emitting region does not introduce significant extra lag time. As we will show in section 5, the observed lag time in each energy bin is the proportional to the true lag time multiplied by the line flux. Thus, if different energy bins have nearly the same true lag time, the line profile in the lag spectrum is similar to that in the flux spectrum. In this sub-section, we show that $K\alpha$ photons bouncing between the inner surface of the funnel wall also cause broadening but with significant extra lag.

Consider a conical wall of opening angle $\alpha_c \lesssim 30^\circ$ moving radially outwards at velocity β (and $\gamma = 1/\sqrt{1-\beta^2}$). At point \mathcal{A} , we assume that a $K\alpha$ photon is emitted along the local surface normal. The energy of this photon in the BH frame is $\epsilon = \epsilon_0/\gamma$, where ϵ_0 is the rest line energy. We assume that the photon is immediately reflected when it reaches the other side of the wall at point \mathcal{B} . The angle between the momentum vectors of the photon and the electron at point \mathcal{B} is $\phi = \pi/2 - 2\alpha_c$. In the electron's comoving frame, the photon's energy is $\epsilon' = \epsilon\gamma(1 - \beta \cos \phi)$. We assume that the photon is scattered toward the direction of the observer (along the jet axis) and ignore electron's recoil, so the scattered photon's energy in the BH rest frame will be

$$\epsilon_{\text{obs}}^{\mathcal{B}} = \frac{\epsilon'}{\gamma(1 - \beta \cos \alpha_c)} = \frac{\epsilon_0(1 - \beta \sin 2\alpha_c)}{\gamma(1 - \beta \cos \alpha_c)}. \quad (10)$$

Note that if the photon were initially emitted from point \mathcal{A} directly toward the observer, its energy is

$$\epsilon_{\text{obs}}^{\mathcal{A}} = \frac{\epsilon_0}{\gamma(1 - \beta \cos \alpha_c)}. \quad (11)$$

From eqs. (10) and (11), we see that the energy of the photon after bouncing ($\epsilon_{\text{obs}}^{\mathcal{B}}$) is a factor of $(1 - \beta \sin 2\alpha_c)$ smaller than that without bouncing ($\epsilon_{\text{obs}}^{\mathcal{A}}$). For typical parameters ($\alpha_c \sim 20^\circ-30^\circ$, $\beta \sim 0.1-0.2$), we have $\epsilon_{\text{obs}}^{\mathcal{A}}/\epsilon_{\text{obs}}^{\mathcal{B}} - 1 \in (6\%, 17\%)$. We assume point \mathcal{A} is at distance R from the BH, so the extra lag due to bouncing in this case is

$$\Delta t_{\text{lag}} = \frac{R}{c} \tan 2\alpha_c (1 - \sin \alpha_c). \quad (12)$$

For $\alpha_c = 20^\circ$ (30°), we obtain $\Delta t_{\text{lag}} \simeq 1.8 \times 10^3 R_{14}$ s ($2.9 \times 10^3 R_{14}$ s).

The estimates above are based on the assumption that the photon is emitted along the surface normal at point \mathcal{A} . To model the line profile in detail, one needs to consider a more realistic geometry with an extended emitting region and then take into account beaming at the emitting point and electrons' recoil (and possible absorption) at the scattering point. Instead of going into these details, here we only comment on the qualitative picture that each bounce broadens the line by ~ 1 keV and causes extra lag time of ~ 2000 seconds. Later in section 5, we show that the red wing of the lag-energy spectrum from *XMM-Newton* is qualitatively consistent with broadening due to bouncing.

4.4 Blueshift due to the radiation-driven wind

Absorption and scattering of γ/X -rays striking the surface of the envelope also deposit into the surrounding gas a component of momentum parallel to the surface. This momentum accelerates a layer of gas near the surface of the envelope with Thomson depth $\tau_{\text{atm}} \sim 3$ (what we call the *atmosphere*, see Fig. 1), and the rate of acceleration is

$$g_{\parallel} = \frac{\eta_{\text{rel}} L \sin^2 \theta}{4\pi \varrho^2} \frac{\kappa_T}{c\tau_{\text{atm}}} \cos(\theta - \alpha_c), \quad (13)$$

where L is the isotropic-equivalent bolometric luminosity (including γ -rays), κ_T is the Thomson opacity and ϱ is the cylindrical radius of the gas from the jet axis. We assume the acceleration operates from $R = \varrho/\sin \alpha_c$ to $2R$ and obtain

⁷ A Gaussian fit with standard deviation 0.67 keV and FWHM = 1.6 keV was obtained by Kara et al. (2016), but the fit was poor due to the asymmetric line shape (strong red wing with little blue wing). The point with half of the peak lag time is about 1 keV below the peak energy.

the asymptotic speed $v \simeq (g_{\parallel} R)^{1/2}$, i.e.

$$v \simeq 0.3c \left(\frac{\eta_{\text{rel}} L_{47.5}}{0.1 R_{14}} \frac{3}{\tau_{\text{atm}}} \right)^{1/2} \frac{\sin \theta}{\sin \alpha_c} [\cos(\theta - \alpha_c)]^{1/2}. \quad (14)$$

Since $\alpha_c \simeq \theta \ll 1$, the trigonometry factor is $\simeq 1$. Therefore, we find that the γ /X-ray flux required to generate the $K\alpha$ photons can naturally accelerate the $K\alpha$ -emitting gas to the speed required by the $K\alpha$ blueshift, 0.1-0.2 c . The gas at the funnel wall may be further accelerated to higher speeds after passing through the $K\alpha$ production region.

5 $K\alpha$ LAG TIME

The lag-energy spectrum of Swift J1644+57 shows that the variations of Fe $K\alpha$ line flux at frequencies $\nu_{\text{var}} = (2-10)(1+z) \times 10^{-4}$ Hz follow the corresponding variations of the continuum at 4-5 keV and 8-13 keV by a time lag of $t_{\text{obs}} \sim 120/(1+z)$ s (with 1- σ error ~ 40 s). The requirement that the fluorescing gas must be at a distance $\gtrsim 10^{14}$ cm seems in conflict with this short lag time. However, in this section, we show that the measured lag time suffers from significant dilution due to the coherently varying continuum component. The dilution-corrected lag time constrains the radius where the jet radiation is produced.

We denote the ratio between the $K\alpha$ flux and the direct continuum flux in the peak lag-time energy bin 7.4-8.1 keV as q , and the dilution of lag time depends on q . Since the direct continuum flux dominates each energy bin, we have $q \ll 1$. Consider the superposition of a continuum component $\sin \omega t$ and a reflected component delayed by t_{true} with a much smaller amplitude $q \sin \omega(t - t_{\text{true}})$, i.e.

$$\sin \omega t + q \sin \omega(t - t_{\text{true}}) = A \sin \omega(t - B t_{\text{true}}). \quad (15)$$

It is straightforward to show that

$$A = (1 + 2q \cos \omega t_{\text{true}} + q^2)^{1/2}, \quad (16)$$

$$B = \frac{1}{\omega t_{\text{true}}} \tan^{-1} \frac{q \sin \omega t_{\text{true}}}{1 + q \cos \omega t_{\text{true}}},$$

and B is the ratio between the observed (diluted) lag time t_{obs} and the true lag time t_{true} . Note that a component that does not vary in the $(2-10)(1+z) \times 10^{-4}$ Hz frequency range has no effect on the measured lag, because it is filtered out in the cross-correlation process in this specific frequency range (Uttley et al. 2014). In the limit of $q \ll 1$, we have

$$\frac{t_{\text{obs}}}{t_{\text{true}}} = B \simeq q \text{sinc}(2\pi \nu_{\text{var}} t_{\text{true}}) \quad (17)$$

where ν_{var} is the frequency of flux variations and we have used the function $\text{sinc}(x) = \sin x/x$.

In section 4, we have estimated $EW \sim 400 \bar{\eta}_{\text{rel}}$ eV with an uncertainty of a factor of $\lesssim 3$, where $\bar{\eta}_{\text{rel}}$ is the X-ray intensity correction due to relativistic beaming averaged over the reprocessing surface and $\bar{\eta}_{\text{rel}} \lesssim 0.2$ is required by the Fe ionization state. Hereafter, we suppose that the EW of the broad $K\alpha$ line is $\lesssim 80$ eV, so the ratio between the line and continuum fluxes in the 7.4-8.1 keV energy bin has an upper limit (from assuming all $K\alpha$ photons to be in this bin)

$$q \lesssim \frac{EW}{0.7 \text{ keV}} \lesssim 0.1 \quad (18)$$

Since $\text{sinc}(2\pi \nu_{\text{var}} t_{\text{true}}) < 1$, we obtain from eq. (17) a lower limit of the true lag time $t_{\text{true}} \gtrsim 8 \times 10^2$ s.

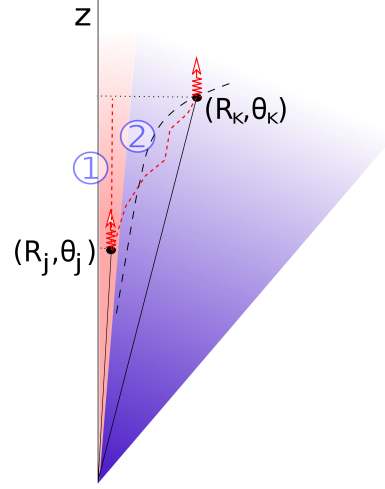


Figure 3. Schematic picture of Fe $K\alpha$ line production in the jet-envelope interaction geometry. We use spherical polar coordinates centered on the BH with polar/ z axis pointing toward the observer. The positions of the jet radiation and $K\alpha$ emission are (R_j, θ_j) and (R_K, θ_K) , respectively. The true lag time between the continuum and $K\alpha$ line is light-travel time difference between the two paths marked in dashed red curves. The black dashed curve is the Thomson surface where the optical depth for electron scattering $\tau = 1$.

In the lag-energy spectrum, the measured lag time drops toward the red wing. Broadening due to bouncing between the funnel wall surface causes longer lag time, and hence the flux ratio q must decrease toward the red wing faster than the increasing of lag time. From §4.3, we see that bouncing between the funnel wall surface causes broadening of ~ 1 keV and extra lag time $\Delta t_{\text{lag}} \sim 2 \times 10^3$ s. The lag-energy spectrum has rather poor energy resolution and the half-lag point (where the measured lag is half of the peak lag) is roughly ~ 1 keV below the peak. The line-to-continuum flux ratio at the half-lag point $q_{1/2}$ is smaller than the ratio at the peak q (eq. 18) by a factor of $t_{\text{true}}(\text{peak})/2\Delta t_{\text{lag}} \gtrsim 0.2$ (using $t_{\text{true}}(\text{peak}) \gtrsim 8 \times 10^2$ s), i.e. $q_{1/2} \gtrsim 0.2q$. This is qualitatively consistent with the fact that broadening due to bouncing decreases the line flux density.

Modeling the lag-energy spectrum in detail is out of the scope of current work, but we emphasize the following two points: (1) scattering off the funnel wall causes photon energy redshift from the line center and introduces extra lag time; (2) the line amplitude in the lag-energy spectrum is proportional to the product of the number of $K\alpha$ photons and their lag time, while the flux-spectrum amplitude is proportional only to the number of $K\alpha$ photons. Therefore, the line in the lag-energy spectrum is broader than that in the flux spectrum.

In the following, we use the true lag time to constrain the jet radiation radius. Let us assume the positions of direct continuum and $K\alpha$ emission are (R_j, θ_j) and (R_K, θ_K) respectively in spherical polar coordinates as shown in Fig.

(3). The light-travel time for direct continuum is

$$t_1 = (R_K \cos \theta_K - R_j \cos \theta_j)/c \simeq (R_K \cos \theta_K - R_j)/c \quad (19)$$

where we have used $\cos \theta_j \approx 1$. The light-travel time for diffusion plus advection in the envelope t_2 depends on the detailed velocity and density profile of the envelope, but a simple estimate can be made as follows. In the optically thin limit $\tau \sim 1$, photons travel almost in a straight line, i.e.

$$t_2 \simeq (R_K^2 + R_j^2 - 2R_K R_j \cos \theta_K)^{1/2}/c, \quad (20)$$

where we have used $\theta_j \ll \theta_K$. Using $R_K = xR_j$, we have

$$t_2 - t_1 \simeq (\sqrt{x^2 - 2x \cos \theta_K + 1} - x \cos \theta_K + 1)R_j/c, \quad (21)$$

which depends on x weakly. It varies in $(0.25, 0.5)R_j/c$ or $(0.5, 1.0)R_j/c$ when $x \in (1.5, 7)$ for $\theta_K = 20^\circ$ or 30° respectively, so we obtain

$$t_2 - t_1 \simeq R_j/2c, \text{ if } \tau \sim 1. \quad (22)$$

On the other hand, when the optical depth of the line production region is large $\tau \gg 1$, photons undergo many scatterings $N \sim \tau$ and hence travel slower than free streaming. Photons are either advected by the fluid motion (if $\tau > 1/\beta$) or diffuse through the envelope (if $\tau < 1/\beta$), and in any of the two cases, a conservative estimate of the travel time is the diffusion time⁸

$$t_2 \simeq \tau R_j/2c, \text{ if } \tau \gg 1. \quad (23)$$

Combining eq. (22) and (23), we obtain the true lag time expected from the jet-envelope interaction

$$t_{\text{true}} = t_2 - t_1 \simeq \tau R_j/2c, \text{ for any } \tau \gtrsim 1, \quad (24)$$

which gives $\tau R_j \simeq 5 \times 10^{13} (t_{\text{true}}/8 \times 10^2 \text{ s}) \text{ cm}$. Since $t_{\text{true}} \gtrsim 8 \times 10^2 \text{ s}$ and $\tau \sim 3$, we obtain a lower limit of the jet radiation radius of $\sim 2 \times 10^{13} \text{ cm}$. On the other hand, as we show in Appendix A, the photospheric radius of the envelope is typically \sim a few $\times 10^{14} \text{ cm}$, which gives an upper limit of the jet radiation radius of $\sim 3 \times 10^{14} \text{ cm}$. We conclude that the radius where the jet energy is converted to radiation is $2 \times 10^{13} \lesssim R_j \lesssim 3 \times 10^{14} \text{ cm}$.

6 DISCUSSION

In this section, we discuss the implications of our results for a variety of topics, including the radiation mechanism of γ /X-rays, other observable signatures of jet-envelope interaction, and a possible explanation of the late-time radio emission from Swift J1644+57. Some remaining issues and caveats are mentioned at the end.

(1) Many different radiation mechanisms for the γ /X-ray continuum in Swift J1644+57 have been discussed by Crumley et al. (2016). The leading candidates are synchrotron emission from electrons accelerated by magnetic reconnection and the external radiation being inverse-Compton scattered by electrons in the jet (hereafter EIC model). Lu & Kumar (2016) showed that the EIC model

is consistent with Swift J2058+05 where the thermal external radiation field was observed in the UV-optical. An issue of the EIC model is how to produce a power-law γ /X-ray spectrum, because hot electrons cool down to Lorentz factors $\gamma_e \sim 1$ extremely quickly. Here we discuss the implications of the results from this work on the EIC model. The general idea is that multiple scattering within a flow that has strong shear motion can produce a power-law spectrum in a Fermi-like process. The number of leptons per proton⁹ is denoted as $\xi_e \in [1, m_p/m_e]$ and the magnetization parameter is σ . If the jet has isotropic equivalent power $L_j = 10^{48} L_{j,48} \text{ erg s}^{-1}$, Lorentz factor $\Gamma = 10\Gamma_1$ and half-opening angle $\theta_j = 0.1\theta_{j,-1}$, electron number density at radius $R = 10^{14} R_{14} \text{ cm}$ is $n_e = L\xi_e/[4\pi R^2 \Gamma m_p c^3 \max(1, \sigma)]$ (in the BH's rest frame), so the jet optical depth in the transverse direction is

$$\tau_{j,\text{trvs}} \simeq \sigma_T n_e R \theta_j \simeq 0.12 \frac{L_{j,48} \theta_{j,-1} \xi_e}{R_{14} \Gamma_1 \max(1, \sigma)}, \quad (25)$$

and the optical depth for a photon propagating in the radial direction outward is a factor of ~ 10 smaller.

The fraction of the jet radiation impinging the surface of the envelope is

$$f_{\text{imp}} = \frac{\int_{\alpha_c}^{\pi/2} \frac{dL}{d\Omega}(\theta) \sin \theta d\theta}{\int_0^{\pi/2} \frac{dL}{d\Omega}(\theta) \sin \theta d\theta} \sim \bar{\eta}_{\text{rel}}. \quad (26)$$

This estimate is a consequence of the fact that $dL/d\Omega(\theta)$ is a rapidly-declining function of θ . Because $\eta_{\text{rel}}(\theta) \equiv [dL/d\Omega(\theta)]/(dL/d\Omega|_{\text{LOS}})$ is the X-ray intensity correction due to relativistic beaming, we have $\int_{\alpha_c}^{\pi/2} dL/d\Omega \sin \theta d\theta \sim dL/d\Omega|_{\text{LOS}} \bar{\eta}_{\text{rel}} \alpha_c^2/2$. The LOS of the observer is close to the jet axis and most radiation power is beamed within the opening cone of angle α_c , so the denominator is $\sim dL/d\Omega|_{\text{LOS}} \alpha_c^2/2$, and hence $f_{\text{imp}} \sim \bar{\eta}_{\text{rel}}$. This means roughly a fraction of $\sim 10\% \bar{\eta}_{\text{rel},-1}$ of the beaming corrected jet radiation energy is reprocessed by the surrounding envelope.

Consider a fraction $f_{\text{imp}} \sim \bar{\eta}_{\text{rel}}$ of the photons that have been scattered once by the jet impinging on the surrounding gas again. When the ionization parameter is high $\xi > 10^3 \text{ erg cm s}^{-1}$, the albedo in the 0.3-10 keV range of is of order unity (Lightman & White 1988), so most of the photons are reflected back to the jet region and will likely get scattered again by the jet electrons. If electrons in the jet are cold ($\gamma_e \sim 1$), photons scattered by the jet obtain a fractional energy gain of Γ_r^2 , where $\Gamma_r \simeq \Gamma \Gamma_s (1 - \beta_s)$ is the relative Lorentz factor between the jet (Lorentz factor Γ) and the reflecting gas at the Thomson surface (speed β_s and Lorentz factor Γ_s).

Therefore, the Compton y parameter for repetitive scat-

⁸ Consider a photon in a 3D random walk with step sizes in Poisson distribution of mean value λ (mean free path). The mean distance traveled after N steps is $S_N = \sqrt{2N}\lambda$ and the mean travel time is $t_N = N\lambda/c = S_N^2/(2\lambda c)$.

⁹ We assume that the jet kinetic energy is dominated by protons. If the kinetic energy is dominated by e^\pm pairs, the optical depth for annihilation at the base of the jet is $\sim \chi m_p/(\sigma_0 m_e)$, where σ_0 is the initial magnetization and χ is the ratio between true jet power and the Eddington luminosity and we have assumed Thomson cross-section because relativistic leptons cool rapidly via synchrotron process. For Swift J1644+57, we have $\chi \sim 10$ -100 (depending on the radiation efficiency), so pairs will annihilate after jet launching if $\sigma_0 \lesssim 10^4$. Pair plasma also suffers from a much stronger Compton drag that may slow down the jet quickly.

tering between the jet and surrounding envelope is

$$y \simeq \bar{\eta}_{\text{rel}} \tau_{j,\text{trvs}} \Gamma_r^2 \simeq 0.6 \frac{\bar{\eta}_{\text{rel},-1} L_{j,48} \xi_e}{R_{14} \max(1, \sigma)} \frac{\Gamma_s^2 (1 - \beta_s)^2}{0.5} (\Gamma \theta_j), \quad (27)$$

from which we see that y is of order unity for a baryonic jet at radius $R \sim 10^{14}$ cm, so a power-law spectrum may be produced in the EIC model even when the jet electrons are cold. Recall that in the model of [Kara et al. \(2016\)](#) the source is moving sub-relativistically, and relativistic power-law electrons are required to produce the observed hard power-law γ /X-ray spectrum. The thermal seed photons from the surrounding envelope have energy density $\sim aT^4 \sim 10^6$ erg cm $^{-3}$ for $T = 10^5$ K, which means the inverse-Compton cooling time of an electron with Lorentz factor $\gamma_e \gg 1$ is very short: $\sim 30\gamma_e^{-1}$ s. Here, the EIC model with cold electrons does not have the cooling problem. The isotropic equivalent EIC luminosity from a baryonic jet with cold electrons is given by

$$L_{\text{EIC}} \sim \frac{L_j R/c}{\Gamma m_p c^2} \times \sigma_{\text{T}} c \Gamma^2 a T^4 \sim (3 \times 10^{47} \text{ erg s}^{-1}) L_{j,48} R_{14} \Gamma_1 T_5^4, \quad (28)$$

which is consistent with the observed γ /X-ray luminosity in the first ~ 10 d ([Burrows et al. 2011](#); [Bloom et al. 2011](#)). Note that the jet optical depth in the transverse direction ($\tau_{j,\text{trvs}}$, eq. 25) drops dramatically when photon energies in the jet comoving frame approach the Klein-Nishina regime ($h\nu' \sim m_e c^2$), so the power-law spectrum cuts off at \sim a few MeV in the EIC model. This could be tested by future observations.

(2) In order for the surface of the envelope not to be over-ionized, the ratio between the X-ray intensity striking the surface and the intensity beamed in the direction of the observer is $\bar{\eta}_{\text{rel}} \lesssim 0.2$. However, we did not specify how the angle-dependent radiation power distribution $dL/d\Omega(\theta)$ is physically realized. One scenario is that the jet has a core-sheath structure, i.e. an ultra-relativistic core is surrounded by a mildly relativistic sheath with $\Gamma_{\text{sh}} \sim 2$ (e.g. [Georganopoulos & Kazanas 2003](#); [Giroletti et al. 2004](#); [Ghisellini et al. 2005](#)), so the sheath scatters the narrowly beamed radiation from the core to much wider angles. Another possibility is that the jet has Lorentz factor of $\Gamma \sim 3$ -5 but the opening angle of the jet is much narrower than $1/\Gamma$. This allows a significant fraction of jet radiation to impinge on the surrounding optically thick gas, and at the same time direct hydrodynamical contact between the jet and envelope (baryon pollution) is avoided. The third scenario is that, although the bulk motion of the jet has a large Lorentz factor $\Gamma \sim 10$, magnetic reconnection at the jet dissipation radius produces relativistic motion in the jet comoving frame (e.g. [Narayan & Kumar 2009](#); [Giannios et al. 2009](#)). This allows the relativistic beaming angle to be much wider than $1/\Gamma$. The results in this work do not depend on how the angle dependence of the jet radiation is physically realized, as long as the beaming correction $\bar{\eta}_{\text{rel}} \lesssim 0.2$.

(3) The total amount of radiation power reprocessed by the surrounding envelope is given by

$$L_{\text{imp}} = f_{\text{imp}} \int_0^\pi \frac{dL}{d\Omega}(\theta) \sin \theta d\theta \sim \bar{\eta}_{\text{rel}} \alpha_c^2 \left. \frac{dL}{d\Omega} \right|_{\text{LOS}} \sim (7 \times 10^{44} \text{ erg s}^{-1}) \left(\frac{\alpha_c}{30} \right)^2 \bar{\eta}_{\text{rel},-1} L_{47.5}, \quad (29)$$

where we have used $\int_0^\pi dL/d\Omega \sin \theta d\theta \sim dL/d\Omega|_{\text{LOS}}$, α_c^2 , $f_{\text{imp}} \sim \bar{\eta}_{\text{rel}}$, and $L = 4\pi dL/d\Omega|_{\text{LOS}} = 10^{47.5} L_{47.5}$ erg s $^{-1}$ is the isotropic equivalent bolometric luminosity from the jet. In the momentum-driving limit (eq. 13), the expanding atmosphere only carries a small fraction of the energy of the reprocessed jet radiation. The γ /X-rays may be advected out with the outflow or bounce between the inner walls until the photons' momenta are directed within the narrow opening angle of the funnel wall, and in this process they could get absorbed (bound-free absorption) or Compton down-scattered. For example, a photon of energy $\epsilon = m_e c^2/N$ loses most of its energy to electrons after $\sim N$ scatterings. The energy of the reprocessed jet radiation is converted to gas internal energy which is then converted to bulk kinetic energy via adiabatic expansion. This energy-driven wind likely involves more envelope mass and is wider than the momentum-driven one. The power of the energy-driven wind could be a large fraction of L_{imp} given in eq. (29), and hence it may be much stronger than the possible wind launched from the accretion disk. If all jetted TDEs have jet-envelope interactions similar to the one we propose for Swift J1644+57, their UV-optical emission may be systematically brighter than in non-jetted TDEs. If the observer's LOS is within the cone of the reprocessing wall, the thermal UV-optical emission due to the reprocessed jet radiation has temperature $T \sim [L_{\text{imp}}/(4\pi R^2 \sin^2 \alpha_c \sigma_{\text{SB}})]^{1/4} \sim (1.4 \times 10^5 \text{ K}) \bar{\eta}_{\text{rel},-1}^{-1/4} L_{47.5}^{1/4} R_{14}^{-1/2}$, where σ_{SB} is the Stefan-Boltzmann constant. The temperature and luminosity will be lower for off-axis observers.

(4) The radio emission from Swift J1644+57 was from the external shocks produced when the jet and possibly a wind interacted with the circum-nuclear medium (CNM) at large distances from the BH. The radio lightcurve and spectrum in the first few weeks can be adequately explained by the external shocks from a relativistic jet of Lorentz factor ~ 10 ([Metzger et al. 2012](#)). In their model, the CNM density decreases with radius rapidly $n \propto r^{-2}$. Since no indication of significant late-time energy injection into the jet was seen in the X-ray lightcurve, as the jet-driven shock decelerates, its radio emission should fade away after ~ 30 d. However, an unexpected rebrightening phase was found at ~ 150 d post-discovery, which may be due to a slower non-/mildly-relativistic wind ([Berger et al. 2012](#); [Zauderer et al. 2013](#); [Barniol Duran & Piran 2013](#); [Mimica et al. 2015](#)), although [Kumar et al. \(2013\)](#) had a different explanation. Here, we propose that the jet-envelope interaction naturally launches a wide-angle non-relativistic wind, which drives an external forward shock capable of explaining the radio rebrightening.

The emission from the forward shock roughly peaks at the deceleration radius R_{dec} where the swept-up mass equals to the ejecta mass. For the purpose of a rough estimate, we assume the CNM density profile in Swift J1644+57 to be similar to our Galactic Center $n(R) = n_{\text{pc}}(R/\text{pc})^{-1.5}$ and $n_{\text{pc}} = 10n_{\text{pc},1}$ cm $^{-3}$ ([Baganoff et al. 2003](#)). If the wind has kinetic energy E_w and speed $\beta_w c$, the deceleration radius is $R_{\text{dec}} \simeq (0.03 \text{ pc}) E_{w,51}^{2/3} (\beta_w/0.3)^{-4/3} n_{\text{pc},1}^{-2/3}$, so the deceleration time is $t_{\text{dec}} \simeq R_{\text{dec}}/(\beta_w c) \simeq (100 \text{ d}) E_{w,51}^{2/3} (\beta_w/0.3)^{-7/3} n_{\text{pc},1}^{-2/3}$. The emission from external shocks has been well studied in the gamma-ray burst literature and it is generally assumed that power-law electrons and magnetic fields share fractions of ϵ_e and ϵ_B of

the thermal energy in the shocked region (e.g. Kumar & Zhang 2015). The forward shock accelerates swept-up electrons to a power-law distribution $dN/d\gamma_e \propto \gamma_e^{-p}$ with minimum Lorentz factor $\gamma_m = (p-1)\epsilon_e m_p \beta_w^2 / [2(p-2)m_e] \simeq 30 \epsilon_{e,-1} (\beta_w/0.3)^2$ for $p = 2.4$, which is given by the high-frequency radio spectrum $F_\nu \propto \nu^{-0.7} = \nu^{(1-p)/2}$. At the deceleration radius, the magnetic field strength in the shocked region is $B = (0.1 \text{ G}) \epsilon_{B,-2}^{1/2} (\beta_w/0.3)$. The synchrotron emission from an electron with Lorentz factor γ_e peaks at $\nu = 3\gamma_e^2 eB / (4\pi m_e c) \simeq (4.2 \text{ GHz}) \gamma_{e,2}^2 B_{-1}$ and the peak specific power is $P_{\nu,\text{peak}} \simeq e^3 B / (m_e c^2)$.

The late-time radio spectrum peaks at $\sim 10 \text{ GHz}$ and roughly has $F_\nu \propto \nu^2$ below the peak frequency (Berger et al. 2012). The synchrotron frequency associated with γ_m is much below GHz, so the peak corresponds to the self-absorption frequency ν_a (associated with Lorentz factor γ_a) roughly given by $4\pi R_{\text{dec}}^2 2kT_a \nu_a^2 / c^2 \simeq N(\geq \gamma_a) P_{\nu,\text{peak}} / (4\pi)$, where $kT_a = \gamma_a m_e c^2$ is the temperature associated with the emitting electrons. The number of electrons emitting at frequency ν_a is $N(\geq \gamma_a) \simeq 2E_w / (\beta_w^2 m_p c^2) (\gamma_a / \gamma_m)^{1-p}$. Therefore, we obtain the self-absorption frequency $\nu_a \simeq (6 \text{ GHz}) E_{w,51}^{-0.1} (\beta_w/0.3)^{1.8} n_{\text{pc},1}^{0.4} \epsilon_{B,-2}^{0.7} \epsilon_{e,-1}^{0.4}$ and the peak flux density $F_{\nu_a} \simeq (7 \text{ mJy}) E_{w,51}^{1.1} (\beta_w/0.3)^{1.3} n_{\text{pc},1}^{-0.3} \epsilon_{B,-2}^{0.6} \epsilon_{e,-1}^{1.1}$ (for $z = 0.354$). To within a factor of $\lesssim 3$, these estimates roughly agree with the radio data after about 90 d (Berger et al. 2012) when the jet-driven external shocks have faded away. Better agreement can be comfortably made by adjusting some of the parameters such as ϵ_B and ϵ_e . For more detailed modeling, one needs to consider many uncertain factors: the angular distribution of wind energy/speed, the unknown CNM density profile, and electron acceleration and magnetic field amplification at collisionless shocks.

(5) Due to the uncertainty and complexity of the system, our jet-envelope interaction model is limited in the following two aspects. First, we only consider the impact of the jet radiation on the surrounding envelope and have ignored the feedback on the jet. In reality, the jet and envelope may be dynamically coupled through the effective viscosity provided by Compton scattering. Second, the detailed $K\alpha$ line production and radiative transfer processes (e.g. line flux profile, lag-energy profile) have not been studied. Our model can be improved by future numerical simulations of jet-envelope coupling and will be tested by future observations of jetted TDEs.

7 CONCLUSION

If the γ /X-rays from jetted TDEs are produced below the photospheric radius of the surrounding optically thick envelope, a fraction of the jet radiation may interact with and affect the dynamics of the envelope. An evidence of this interaction is the Fe $K\alpha$ line detected in the reverberation lag spectrum from Swift J1644+57 by Kara et al. (2016).

The discovery paper argued that the source of the γ /X-ray continuum was located very close to the BH (~ 30 gravitational radii) and moved sub-relativistically. We have re-analyzed the lag spectrum, pointing out that dilution effects cause it to indicate a geometric scale an order of magnitude larger than inferred by Kara et al. (2016). If the γ /X-ray continuum is produced by a relativistic jet, as suggested by the rapid variability, high luminosity and hard spectrum,

this larger scale predicts an Fe ionization state consistent with efficient $K\alpha$ production. Moreover, the relativistically beamed jet radiation impinging on the funnel wall of the surrounding gas also accelerates the reprocessing layer of Thomson depth $\tau \sim 3$ to speeds $\beta \sim 0.1$ – 0.2 .

Our model can explain the following observational results qualitatively: (i) the line energy is blueshifted from the rest energy ϵ_0 to $\epsilon_{\text{obs}} = \epsilon_0 / [\gamma(1 - \beta \cos \alpha_c)] \simeq (1 + \beta)\epsilon_0$ for funnel wall opening angle $\alpha_c \lesssim 30^\circ$ and outflowing speed $\beta \lesssim 0.2$; (ii) the broad asymmetric red wing in the lag-energy spectrum extending from the peak at $\simeq 8 \text{ keV}$ down to 6–7 keV (energies in the host-galaxy rest frame) is due to $K\alpha$ photons bouncing between the inner surface of the envelope plus Compton down-scattering; (iii) the $K\alpha$ lag time of $\sim 120/(1+z)$ s, which suffers from dilution by the coherently varying continuum photons that dominates in each energy bin, indicates that the jet radiation radius is at $R_j \gtrsim 2 \times 10^{13} \text{ cm}$ (and the photospheric radius of the reprocessing gas gives an upper limit of $R_j \lesssim 3 \times 10^{14} \text{ cm}$).

Our model fits well with the global picture of jetted TDEs. Although our model does not depend on the jet radiation mechanism, we show that the power-law γ /X-rays may be produced by the external photons from the surrounding envelope being repetitively inverse-Compton scattered by cold electrons in the jet. The reprocessed jet radiation drives a non-relativistic wind, which may explain the late-time radio rebrightening of Swift J1644+57. This energy injection may also cause the thermal UV-optical emission from jetted TDEs to be systematically brighter than in non-jetted ones.

8 ACKNOWLEDGEMENTS

We thank the anonymous referee for many useful comments, which improved the content and clarity of the paper. We thank Erin Kara, Chris Reynolds and Phil Uttley for helpful discussion on the $K\alpha$ lag spectrum. We thank Christopher Orban and Lianshui Zhao for help in getting the monoenergetic opacity from the Opacity Project. The idea of a non-relativistic wind possibly causing the radio rebrightening was from discussion with Zhuo Li at Peking University a few years ago. We also thank Sera Markoff for arranging this collaboration. WL is funded by the Named Continuing Fellowship at the University of Texas at Austin. JHK was partially supported by NASA grant NNX14AB43G and by NSF grant AST-1516299. PC acknowledges financial support from the WARP program of the Netherlands Organisation for Scientific Research (NWO).

REFERENCES

- Arcavi, I., Gal-Yam, A., Sullivan, M., et al. 2014, *ApJ*, 793, 38
- Baganoff, F. K., Maeda, Y., et al. 2003, *ApJ*, 591, 891
- Barniol Duran, R., & Piran, T. 2013, *ApJ*, 770, 146
- Berger, E., Zauderer, A., Pooley, G. G., et al. 2012, *ApJ*, 748, 36
- Bloom, J. S., Giannios, D., Metzger, B. D., et al. 2011, *Science*, 333, 203
- Bonnerot, C., Rossi, E. M., Lodato, G., & Price, D. J. 2016, *MNRAS*, 455, 2253

- Bonnerot, C., Price, D. J., Lodato, G., & Rossi, E. M. 2016, [arXiv:1611.09853](#)
- Brown, G. C., Levan, A. J., Stanway, E. R., et al. 2015, *MNRAS*, 452, 4297
- Burrows, D. N., Kennea, J. A., Ghisellini, G., et al. 2011, *Nature*, 476, 421
- Cenko, S. B., Krimm, H. A., et al. 2012, *ApJ*, 753, 77
- Coughlin, E. R., & Begelman, M. C. 2014, *ApJ*, 781, 82
- Coughlin, E. R., Nixon, C., Begelman, M. C., & Armitage, P. J. 2016, *MNRAS*, 459, 3089
- Crumley, P., Lu, W., Santana, R., et al. 2016, *MNRAS*, 460, 396
- Dai, Lixin, McKinney, J.C., & Miller, M.C., *ApJL*, 812, L39
- De Colle, F., Guillochon, J., Naiman, J., & Ramirez-Ruiz, E. 2012, *ApJ*, 760, 103
- Draine, B. T. 2011, *Physics of the Interstellar and Inter-galactic Medium* by Bruce T. Draine. Princeton University Press, 2011. ISBN: 978-0-691-12214-4
- Drenkhahn, G., & Spruit, H. C. 2002, *A&A*, 391, 1141
- Georganopoulos, M., & Kazanas, D. 2003, *ApJL*, 594, L27
- George, I. M., & Fabian, A. C. 1991, *MNRAS*, 249, 352
- Gezari, S., Heckman, T., Cenko, S. B., et al. 2009, *ApJ*, 698, 1367
- Gezari, S., Chornock, R., Rest, A., et al. 2012, *Nature*, 485, 217
- Ghisellini, G., Tavecchio, F., & Chiaberge, M. 2005, *A&A*, 432, 401
- Giannios, D., Uzdensky, D. A., & Begelman, M. C. 2009, *MNRAS*, 395, L29
- Giroletti, M., Giovannini, G., Feretti, L., et al. 2004, *ApJ*, 600, 127
- Granot, J., Komissarov, S. S., & Spitkovsky, A. 2011, *MNRAS*, 411, 1323
- Guillochon, J., & Ramirez-Ruiz, E. 2013, *ApJ*, 767, 25
- Guillochon, J., & Ramirez-Ruiz, E. 2015, *ApJ*, 809, 166
- Guillochon, J., McCourt, M., Chen, X., Johnson, M. D., & Berger, E. 2016, *ApJ*, 822, 48
- Guillochon, J., & McCourt, M. 2016, [arXiv:1609.08160](#)
- Holoien, T. W.-S., Kochanek, C. S., Prieto, J. L., et al. 2016, *MNRAS*, 455, 2918
- Hung, T., Gezari, S., Blagorodnova, N., et al. 2017, [arXiv:1703.01299](#)
- Jiang, Y.-F., Stone, J. M., & Davis, S. W. 2014, *ApJ*, 796, 106
- Jiang, Y.-F., Guillochon, J., & Loeb, A. 2016, [arXiv:1603.07733](#)
- Kara, E., Miller, J. M., Reynolds, C., & Dai, L. 2016, *Nature*, 535, 388
- Kochanek, C. S. 1994, *ApJ*, 422, 508
- Komissarov, S. S., Barkov, M. V., Vlahakis, N., & Königl, A. 2007, *MNRAS*, 380, 51
- Komossa, S., Halpern, J., Schartel, N., et al. 2004, *ApJL*, 603, L17
- Krolik, J. H., & Kallman, T. R. 1987, *ApJL*, 320, L5
- Krolik, J. H., & Piran, T. 2011, *ApJ*, 743, 134
- Krolik, J. H., Piran, T., Svirski, G., & Cheng, R. M. 2016, *ApJ*, 827, 127
- Kumar, P., Barniol Duran, R., Bošnjak, Ž., & Piran, T. 2013, *MNRAS*, 434, 3078
- Kumar, P., & Zhang, B. 2015, *Physics Reports*, 561, 1
- Levan, A. J., Tanvir, N. R., Cenko, S. B., et al. 2011, *Science*, 333, 199
- Levan, A. J., Tanvir, N. R., Brown, G. C., et al. 2016, *ApJ*, 819, 51
- Loeb, A., & Ulmer, A. 1997, *ApJ*, 489, 573
- Lightman, A. P., & White, T. R. 1988, *ApJ*, 335, 57
- Lodato, G., King, A. R., & Pringle, J. E. 2009, *MNRAS*, 392, 332
- Lu, W., & Kumar, P. 2016, *MNRAS*, 458, 1071
- Mangano, V., Burrows, D. N., Sbarufatti, B., & Cannizzo, J. K. 2016, *ApJ*, 817, 103
- Metzger, B. D., Giannios, D., & Mimica, P. 2012, *MNRAS*, 420, 3528
- Metzger, B. D., & Stone, N. C. 2016, *MNRAS*, 461, 948
- Mimica, P., Giannios, D., Metzger, B. D., & Aloy, M. A. 2015, *MNRAS*, 450, 2824
- Narayan, R., & Kumar, P. 2009, *MNRAS*, 394, L117
- Odell, S. L. 1981, *ApJL*, 243, L147
- Pasham, D. R., Cenko, S. B., Levan, A. J., et al. 2015, *ApJ*, 805, 68
- Phinney, E. S. 1982, *MNRAS*, 198, 1109
- Piran, T., Sądowski, A., & Tchekhovskoy, A. 2015, *MNRAS*, 453, 157
- Piran, T., Svirski, G., Krolik, J., Cheng, R. M., & Shiokawa, H. 2015, *ApJ*, 806, 164
- Pozdnyakov, L. A., Sobol, I. M., & Syunyaev, R. A. 1983, *Astrophysics and Space Physics Reviews*, 2, 189
- Sądowski, A., Tejeda, E., Gafton, E., Rosswog, S., & Abarca, D. 2016, *MNRAS*, 458, 4250
- Saxton, C. J., Soria, R., Wu, K., & Kuin, N. P. M. 2012, *MNRAS*, 422, 1625
- Saxton, R. D., Read, A. M., Esquej, P., et al. 2012, *A&A*, 541, A106
- Saxton, R. D., Read, A. M., Komossa, S., et al. 2016, [arXiv:1610.01788](#)
- Schlaflly, E. F., & Finkbeiner, D. P. 2011, *ApJ*, 737, 103
- Shen, R.-F., & Matzner, C. D. 2014, *ApJ*, 784, 87
- Shiokawa, H., Krolik, J. H., Cheng, R. M., Piran, T., & Noble, S. C. 2015, *ApJ*, 804, 85
- Stone, N., Sari, R., & Loeb, A. 2013, *MNRAS*, 435, 1809
- Strubbe, L. E., & Quataert, E. 2009, *MNRAS*, 400, 2070
- Uttley, P., Cackett, E. M., Fabian, A. C., Kara, E., & Wilkins, D. R. 2014, *Astro. Astrophys. Rev.*, 22, 72
- Zauderer, B. A., Berger, E., Soderberg, A. M., et al. 2011, *Nature*, 476, 425
- Zauderer, B. A., Berger, E., Margutti, R., et al. 2013, *ApJ*, 767, 152

APPENDIX A:

We show that the photospheric radius of the envelope responsible for the thermal UV-optical emission is \sim a few $\times 10^{14}$ cm. We define the photospheric radius R_{ph} based on the two observable quantities of a thermal spectrum, bolometric luminosity L_{bol} and temperature T , in the following way

$$L_{\text{bol}} = 4\pi R_{\text{ph}}^2 \sigma_{\text{SB}} T^4, \quad (\text{A1})$$

where σ_{SB} is the Stefan-Boltzmann constant. Note that R_{ph} here does not necessarily equal to the Thomson surface radius R_s where the optical depth for electron scattering τ

Table A1. The photospheric radius defined by $L_{\text{bol}} = 4\pi R_{\text{ph}}^2 \sigma_{\text{SB}} T^4$ can be constrained by eqs. (A5) and (A7) from one data point (ν_0 , $L_0 \equiv \nu_0 L_{\nu_0}$) on the R-J tail at a certain post-discovery time in the host-galaxy rest frame. We list the constraints for some recent TDEs. References: (1) Pasham et al. (2015), (2) Levan et al. (2016), (3) Gezari et al. (2009), (4) Gezari et al. (2012), (5) Holoien et al. (2016).

TDEs	Refs.	ν_0 [Hz]	L_0 [erg/s]	time[d]	R_{min} [cm]	R_{max} [cm]
Sw J2058+05	(1)	1.0e15	1.3e44	11	2.2e14	4.8e14
Sw J1644+57 ^a	(2)	7.1e14	~6.4e43	17	~2.6e14	~6.6e14
D23H-1	(3)	7.5e14	2.9e42	20	3.1e13	1.3e14
D3-13	(4)	8.6e14	9.0e42	~20	4.9e13	1.7e14
PS1-10jh	(4)	4.2e14	5.7e42	30	1.5e14	5.6e14
ASSASN-14li	(5)	9.1e14	9.2e42	8	4.3e13	1.5e14

^a For Swift J1644+57, strong dust extinction causes a large uncertainty (up to a factor of ~ 10 to 30) in the r-band flux, due to unknown reddening $E(B - V)$ and extinction law parameter $R_V \equiv A_V/E(B - V)$. The uncertainties at longer wavelengths are much less ($\sim 50\%$ at H-band), but the near-infrared spectrum before and after extinction correction is clearly not R-J like (there may be a power-law component due to external shocks, see Levan et al. 2016, their Fig. 6). Here, for the purpose of a rough estimate, we apply $R_V = 3.1$ and $E(B - V) = 1.5$ mag to the r-band data and correct for dust extinction of 5.5 mag in the host-galaxy rest frame, using the reddening law calibrated by Schlafly & Finkbeiner (2011). For $R_V = 3.1$ and $E(B - V) = 2$ mag, the photospheric radius is between $R_{\text{min}} = 8.5 \times 10^{14}$ cm and $R_{\text{max}} = 1.6 \times 10^{15}$ cm.

equals to 1. If the bound-free opacity is comparable to electron scattering opacity, thermalization happens near the Thomson surface $R_s \simeq R_{\text{ph}}$.

The peak of the TDE thermal component (at $h\nu \simeq 2.8kT$) is always in the far UV and has never been observed. Therefore, there are large uncertainties in L_{bol} and T and eq. (A1) cannot be directly used to measure R_{ph} . Usually, the observable part is on the Rayleigh-Jeans (R-J) tail

$$\nu L_\nu = \frac{15L_{\text{bol}}}{\pi^4} \left(\frac{h\nu}{kT} \right)^3 = L_0 (\nu/\nu_0)^3, \quad (\text{A2})$$

where we have normalized the spectrum with a measured data point ($\nu = \nu_0$, $\nu L_\nu = L_0$) on the R-J tail. We put L_{bol} from eq. (A1) into eq. (A2), take $\nu = \nu_0$, and then obtain the temperature T as a function of photospheric radius R_{ph}

$$kT = \frac{L_0 c^2}{8\pi^2 \nu_0^3} \frac{1}{R_{\text{ph}}^2} \quad (\text{A3})$$

Since the observed data point is far below the blackbody peak, we have

$$h\nu_0 < kT. \quad (\text{A4})$$

Combining eqs. (A3) and (A4) gives an upper limit of R_{ph} which we denote as R_0 , i.e.

$$R_{\text{ph}} < R_0 \equiv \frac{\sqrt{2} L_0^{1/2} c}{4\pi h^{1/2} \nu_0^2}. \quad (\text{A5})$$

On the other hand, eq. (A2) also gives us the temperature as a function of the bolometric luminosity (ν_0 and L_0 are knowns)

$$kT = \frac{15h\nu_0}{\pi^4 L_0} L_{\text{bol}} \leq \frac{15h\nu_0}{\pi^4 L_0} L_{\text{max}}, \quad (\text{A6})$$

where the maximum bolometric luminosity $L_{\text{max}} \sim 10^{47}$ erg s⁻¹ comes from assuming a total energy budget of $\sim 10^{53}$ erg and the duration of peak luminosity $\sim 10^6$ s.

Then, this upper bound on temperature gives a minimum photospheric radius through eq. (A3). Combining the limits on both ends, we obtain

$$\left(\frac{\pi^4 L_0}{15L_{\text{max}}} \right)^{1/6} < R_{\text{ph}}/R_0 < 1. \quad (\text{A7})$$

For $L_0/L_{\text{max}} = (10^{-2}, 10^{-3}, 10^{-4})$, the left-hand side of eq. (A7) [$\pi^4 L_0/(15L_{\text{max}})$]^{1/6} = (0.63, 0.43, 0.29) is not far from unity. Therefore, we conclude that the photospheric radius defined in eq. (A1) can be constrained to a fairly narrow range $R_{\text{ph}} \in (R_0/3, R_0)$, where R_0 can be determined by one data point (ν_0, L_0) on the R-J tail.

We list in Table A1 the constraints on photospheric radii in some recent TDEs. The jetted TDEs Swift J2058+05, Swift J1644+57 and some non-jetted TDEs have $R_{\text{ph}} \sim$ a few $\times 10^{14}$ cm.